Multiple nutrient stresses at intersecting Pacific Ocean biomes detected by protein biomarkers

Mak A. Saito *et al.*

Science **345**, 1173 (2014);
DOI: 10.1126/science.1256450

12. E. I. Solomon *et al*., *Chem. Rev.* **100**, 235–350 (2000).
13. V. S. Oganesyan, A. J. Thomson, *J. Chem. Phys.* **113**, 5003–5017 (2000).
14. B. P. Gaber, J. P. Sheridan, F. W. Bazer, R. M. Roberts, *J. Biol. Chem.* **254**, 8340–8342 (1979).
15. S. Kathuria, A. C. Martiny, *Environ. Microbiol.* **13**, 74–83 (2011).
16. R. D. Monds, P. D. Newell, J. A. Schwartzman, G. A. O'Toole, *Appl. Environ. Microbiol.* **72**, 1910–1924 (2006).
17. N. H. Williams, A. M. Lebuis, J. Chin, *J. Am. Chem. Soc.* **121**, 3341–3348 (1999).
18. G. Schenk *et al*., *Proc. Natl. Acad. Sci. U.S.A.* **102**, 273–278 (2005).
19. R. D. Cannon, R. P. White, *Prog. Inorg. Chem.* **36**, 195–298 (1988).
20. N. Mitić *et al*., *Chem. Rev.* **106**, 3338–3363 (2006).
21. D. L. Wang, R. C. Holz, S. S. David, L. Que Jr., M. T. Stankovich, *Biochemistry* **30**, 8187–8194 (1991).
22. R. W. Jakuba, J. W. Moffett, S. T. Dyhrman, *Global Biogeochem. Cycles* **22**, GB4012 (2008).
23. C. M. Moore *et al*., *Nat. Geosci.* **6**, 701–710 (2013).
24. M. A. Saito, T. J. Goepfert, J. T. Ritt, *Limnol. Oceanogr.* **53**, 276–290 (2008).
25. J. Wu, W. Sunda, E. A. Boyle, D. M. Karl, *Science* **289**, 759–762 (2000).
26. C. M. Moore *et al*., *Glob. Change Biol.* **12**, 626–634 (2006).

ACKNOWLEDGMENTS

We thank G. O'Toole for providing *P. fluorescens* Pf0-1 genomic DNA; J. Marcoux, B. Pilgrim, and A. Parkin for exploratory experiments; and F. Armstrong, T. Browning, J. McGrady, G. Henderson, D. Herschlag, C. Schofield, A. Thomson, C. Timmel, N. Williams, and R. Williams for valuable discussions. This work was funded by the University of Oxford, Pembroke College Oxford, Oxford Martin School Vaccine Design Institute, the Engineering and Physical Sciences Research Council, the Biotechnology and Biological Sciences Research Council (grant F02150X), and the European Molecular Biology Organization. Structure coordinates and x-ray data have been deposited in the Protein Data Bank with accession codes 4a9v, 4amf, 4alf, and 3zwu.

SUPPLEMENTARY MATERIALS

www.sciencemag.org/content/345/6201/1170/suppl/DC1
Materials and Methods
Figs. S1 to S5
Tables S1 to S4
References (*27*–*44*)

1 April 2014; accepted 7 July 2014
10.1126/science.1254237

MARINE MICROBES

Multiple nutrient stresses at intersecting Pacific Ocean biomes detected by protein biomarkers

Mak A. Saito,[1]* Matthew R. McIlvin,[1] Dawn M. Moran,[1] Tyler J. Goepfert,[1] Giacomo R. DiTullio,[2] Anton F. Post,[3] Carl H. Lamborg[1]

Marine primary productivity is strongly influenced by the scarcity of required nutrients, yet our understanding of these nutrient limitations is informed by experimental observations with sparse geographical coverage and methodological limitations. We developed a quantitative proteomic method to directly assess nutrient stress in high-light ecotypes of the abundant cyanobacterium *Prochlorococcus* across a meridional transect in the central Pacific Ocean. Multiple peptide biomarkers detected widespread and overlapping regions of nutritional stress for nitrogen and phosphorus in the North Pacific Subtropical Gyre and iron in the equatorial Pacific. Quantitative protein analyses demonstrated simultaneous stress for these nutrients at biome interfaces. This application of proteomic biomarkers to diagnose ocean metabolism demonstrated *Prochlorococcus* actively and simultaneously deploying multiple biochemical strategies for low-nutrient conditions in the oceans.

Marine photosynthetic activity in the oceans is largely controlled by nutrient and micronutrient availability. Although this process is critical to marine ecosystem structure, ocean-climate interactions, and nutrient cycling processes, the nutrient-addition incubation experiments typically used to assess which nutrients are limiting are time-intensive and subject to artifacts (*1*), making their deployment to broad geographic regions difficult. Nutrient limitation is commonly parameterized in marine ecosystem and biogeochemistry models so that growth is controlled by the single scarcest nutrient (relative to cellular requirements) (*2*); however, multiple scarce nutrients may also influence phytoplankton community structure (*3*, *4*). Molecular methodologies have shown potential for detecting in situ biomarkers for nutrient stress by measurement of up-regulated transcripts or proteins associated with nutrient scarcity (*5*, *6*), but they can have relatively broad biological specificity and can be difficult to deploy to a wide geographic region (*5*). With advances in mass spectrometry, microbial proteins have begun to be directly measured in complex natural environments; recent metaproteomic surveys of oceanic environments have identified and examined the relative abundance of biogeochemically relevant proteins (*7*, *8*).

In this study, we conducted calibrated quantitative mass spectrometry–based protein biomarker measurements using multiple reaction monitoring (MRM) to characterize nutrient limitation patterns for multiple nutrients on the abundant marine cyanobacterium *Prochlorococcus* (*9*). Samples were collected along a ~4500-km meridional transect through the central Pacific and equatorial Pacific Ocean initiating south of the Hawaiian Islands and ending near the Samoan Islands in October of 2011 (Fig. 1A). The equatorial Pacific is an ideal region to examine the range of nutrient stresses affecting phytoplankton because it crosses several biogeochemical biomes (*10*). Equatorial upwelling caused by Ekman divergence supplies cold, nitrogen-, and phosphorus-rich waters (Fig. 1B and fig. S1) (*11*), resulting in iron limitation of phytoplankton communities (*1*). In contrast, the subtropical gyres to the north and south are highly depleted in multiple nutrients (N, P, and micronutrients; Fig. 1B and fig. S1). The scarcity of multiple nutrients has made it difficult to experimentally determine a single primary limiting nutrient of primary productivity in oligotrophic regions (*3*), and as an alternative, marine ecosystem models have been used to predict iron and nitrogen limitation of the equatorial and subtropical gyre regions of the Pacific, respectively, with a sharp transition between them (*2*, *12*). *Prochlorococcus*, an oxygenic photoautotrophic cyanobacterium, is a major contributor to marine photosynthesis in tropical and subtropical oceanic regions (*1*, *13*) and was observed throughout the transect by its unique divinyl chlorophyll a pigment, particularly in the equatorial upwelling region when total chlorophyll a was also highest (Fig. 1C and fig. S1).

Peptide biomarkers were selected from proteins of interest identified within global metaproteome analyses of the microbial samples taken from this transect. These metaproteome analyses used numerous cyanobacterial genomes and Pacific metagenomes to enable protein identification specific to this region (table S2). Targeted methods were designed using peptide-specific parent to fragment ion transitions (table S3), and synthesized isotope-labeled peptides served as internal standards using MRM on a triple quadrupole mass spectrometer (*14*). Several proteins had been shown in laboratory culture studies of marine cyanobacteria to have potential use as biomarkers of iron and nitrogen stress, including iron deficiency protein IdiA (*5*); flavodoxin, which replaces iron-requiring ferredoxin under iron stress (*15*, *16*); and the global nitrogen response regulator NtcA that serves as a transcriptional activator for alternate forms of nitrogen (such as urea) and is under negative control by ammonium (*17*, *18*). We also targeted the urea transporter of *Prochlorococcus* as an additional nitrogen stress biomarker based on its presence in the metaproteome.

[1]Marine Chemistry and Geochemistry Department, Woods Hole Oceanographic Institution, Woods Hole, MA 02543, USA. [2]College of Charleston, Charleston, SC, USA. [3]Marine Biological Laboratory, Woods Hole, MA 02543, USA.
*Corresponding author. E-mail: msaito@whoi.edu

One challenge in deploying targeted proteomics to the oceans is the reliance of the MRM technique on exact sequence matches, which, in a complex environmental community, can result in the measurement of a subset of a protein's functional sequence diversity (fig. S2). Yet, genomic analysis of cyanobacterial genomes demonstrated that peptides targeted for *Prochlorococcus* nitrogen and iron stress were specific not only

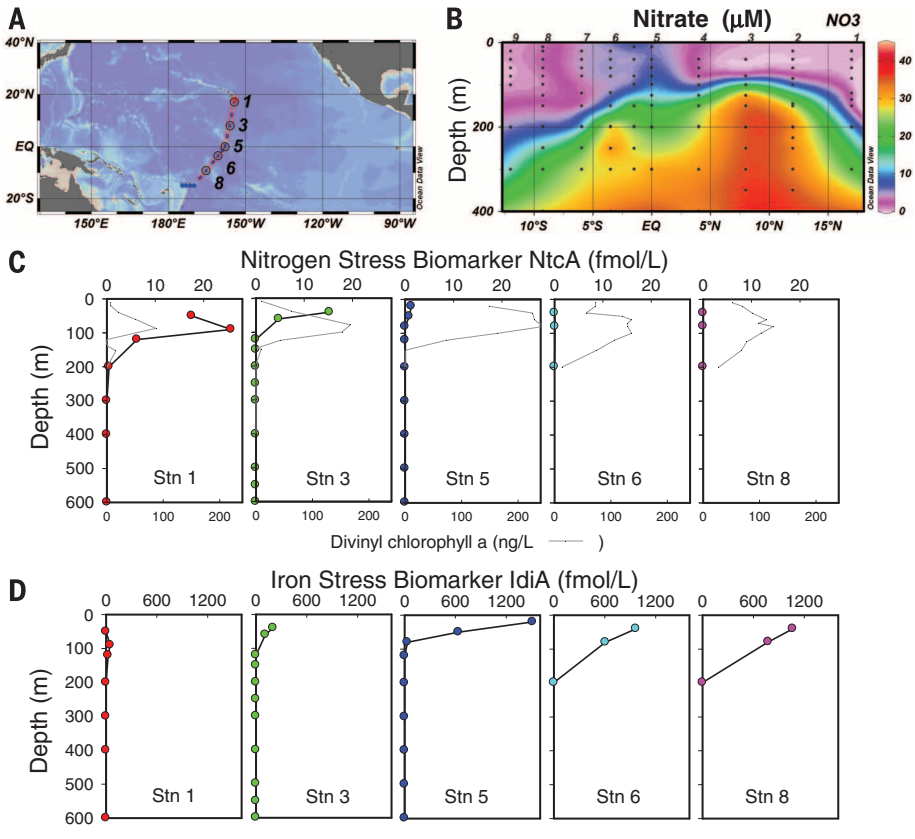

Fig. 1. Station locations, nitrate distributions, and vertical profiles of iron and nitrogen stress biomarkers. (**A**) Cruise track for the METZYME expedition in the central Pacific Ocean aboard the R/V *Kilo Moana* in October 2011 from Hawaii to Samoa (station coordinates in table S1). (**B**) Nitrate distributions along the transect (units of micromolar). Vertical profiles of (**C**) nitrogen and (**D**) iron stress biomarkers NtcA and IdiA, respectively, from the abundant marine cyanobacterium *Prochlorococcus marinus* as measured by targeted proteomics along the transect. With southward progression, a shift in nitrogen to iron stress was observed. Divinyl chlorophyll a distributions are also shown for comparison (in gray). Station 5 was located on the equator. Zero values below the photic zone, where *Prochlorococcus* is absent, demonstrate a lack of false positives.

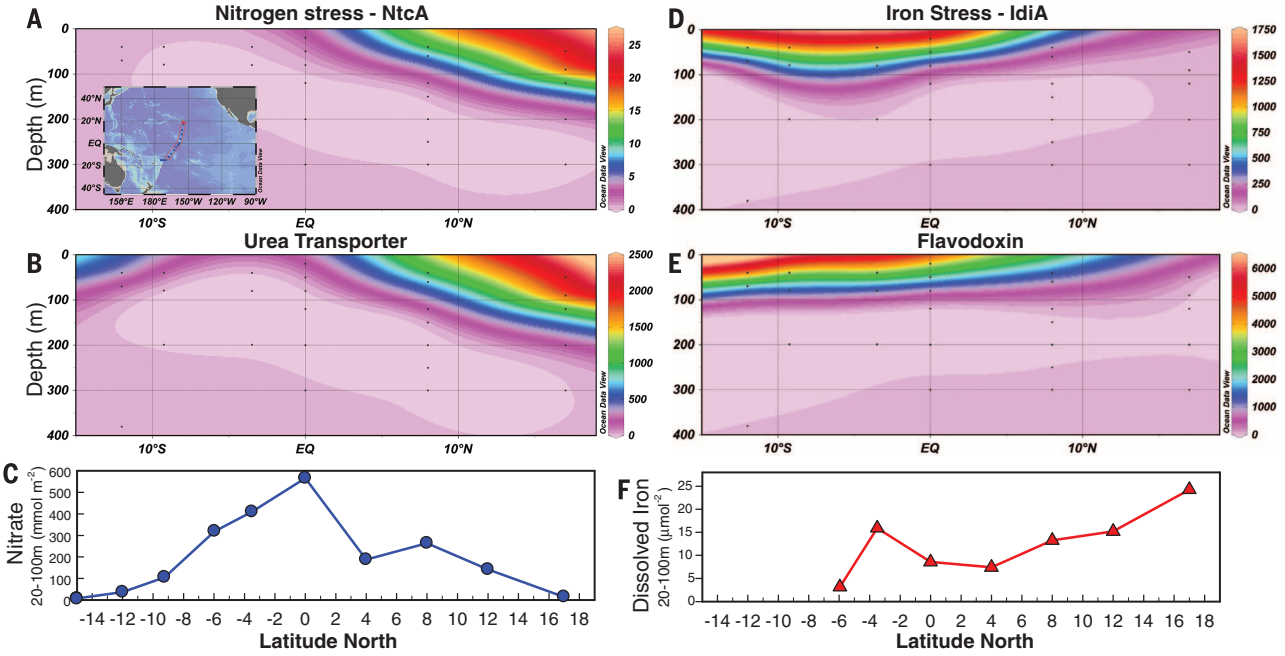

Fig. 2. Ocean sections of *Prochlorococcus* nitrogen and iron metabolic protein biomarkers. (**A** and **B**) NtcA and urea transporter for nitrogen stress in units of fmol/liter (inset: transect station map; peptide IDs 34 and 41 from tables S3 and S4), and (**D** and **E**) IdiA and flavodoxin for iron stress in units of fmol/liter (peptide IDs 27 and 31). (**C** and **F**) Depth-integrated nitrate and dissolved iron for the 20- to 100-m region. At stations 3 and 4, samples were not available at 20 m, so the 40-m values were used as a surface depleted estimate. When no 100-m sample was available, a value was extrapolated from adjacent depths (see table S3).

to the *Prochlorococcus* species, but also showed subspecies specificity to the two currently known high-light ecotypes of *Prochlorococcus* in the upper water column [table S4, the low-B/A I and low-B/A II clades (*19*)], with the exception of one of the two NtcA biomarkers that also targeted the related cyanobacterium *Synechococcus*. Hence, by selecting protein targets identified in metaproteomes that were generated with regional metagenomes and microbial genomes, we could target biomarkers that were representative and abundant for this region. Owing to this subspecies-level resolution, the data presented here are not normalized to *Prochlorococcus* population abundance, because defining and quantifying ecotypes can be challenging. Yet, the unnormalized protein concentration data are of biogeochemical value, as they can be directly related to ecological stoichiometry, nutrient uptake, and enzymatic activity.

The vertical profiles of these biomarker proteins identified a transition between regions of iron and nitrogen stress along the transect (Figs. 1 and 2). Biomarkers for IdiA and flavodoxin went from nondetectable to highly abundant upon entering the equatorial upwelling region as the integrated dissolved iron inventory (from 20 to 100 m) became depleted, from 24 μmol m^{-2} at station 1 to 3 μmol m^{-2} by station 7 (Fig. 2F). This decrease in integrated dissolved iron was observed despite a vertical structure that was more complex than that of nitrate owing to the regional hydrography and long-distance zonal transport of particulate iron (table S5) (*11*, *20*). In contrast, NtcA was abundant in the oligotrophic gyre region of the North Pacific, but became scarce in the equatorial Pacific as the integrated nitrate inventory (20 to 100 m) increased from 4 to 565 mmol m^{-2} (Fig. 2C). Nitrite and ammonia concentrations both increased at the equator and southward (fig. S6), consistent with NtcA distributions. Several criteria corroborate this method for diagnosing the nutritional status of environmental populations of *Prochlorococcus*. First, multiple independent protein biomarkers provided a consistent indication of nutritional stress (NtcA and urea transporter for nitrogen, and IdiA and flavodoxin for iron) and were oceanographically consistent with cyanobacterial proteins being nondetectable below the photic zone. Second, within two of these protein biomarkers, the urea transporter and flavodoxin, multiple peptides were targeted and yielded very similar geographical trends, with variations in abundance likely reflecting the diversity of protein sequence in the natural environment (table S2 and fig. S2). Third, inspection of individual fragmentation patterns (ms^2 spectra) from metaproteomic analyses showed consistent fragment patterns and a lack of interfering ions for the MRM analyses (figs. S3 and S4).

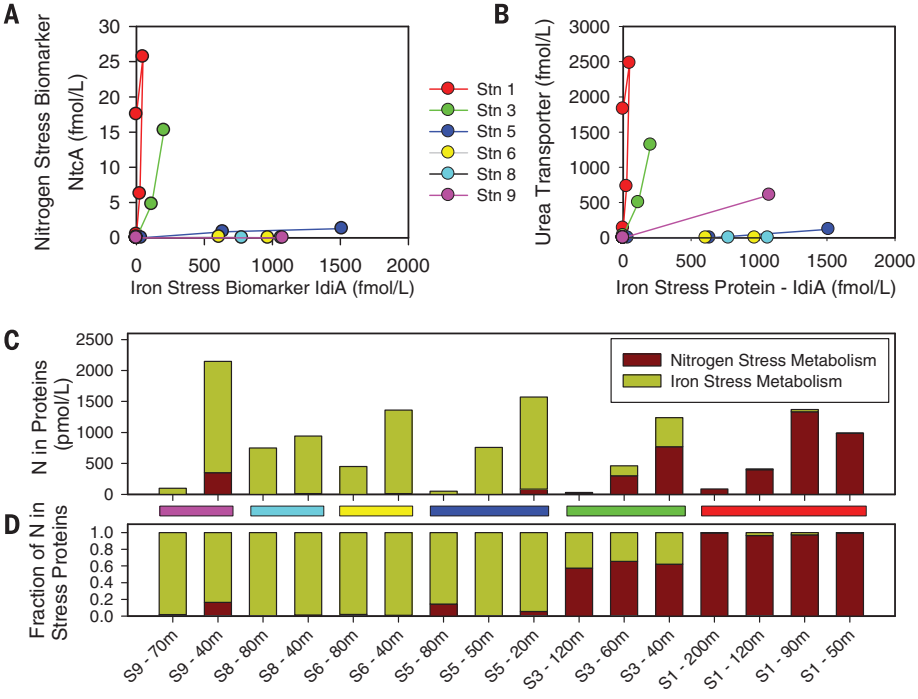

Fig. 3. Comparison of distributions of nitrogen and iron stress biomarkers across the transect. (**A**) Relationships between IdiA and NtcA biomarkers, with shallower depths tending to have increased protein abundances. (**B**) Comparison of distributions of urea transporter abundances and IdiA iron stress biomarker. The coherent ratios for these pairs of biomarkers was indicative of the unique combination of environmental stimuli tuning the protein expression of nutrient-scarcity responses (ratios of biomarkers presented in table S6). (**C**) The nitrogen content within each targeted protein was calculated and summed for selected nitrogen and iron metabolism proteins along the transect (NtcA, urea transporter, and glutamine synthetase for nitrogen metabolism and IdiA and flavodoxin for iron metabolism; peptide IDs 34, 41, 145, 27, 31) and (**D**) represented as a fraction of the total nitrogen for these five proteins. Color bars between (C) and (D) correspond to station symbols in (A) and (B).

Together these biomarker results reveal a gradation of adaptive responses between the NPSG and equatorial regions, with nitrogen and iron stress proteins co-occurring in the transition regions between biomes (Fig. 2). Comparing biomarker abundances with coherent and distinct ratios of NtcA:IdiA and UreA:IdiA peptide abundances at each station (Fig. 3, A and B, and table S6) showed the primary nutrient stress, consistent with previous incubation observations (*26*), yet also revealed co-stresses at biome transitions. Because the protein measurements were calibrated on an absolute scale, we calculated the cellular nitrogen being dedicated to both of these enhanced nitrogen and iron acquisition strategies for five *Prochlorococcus* proteins across this region

These protein biomarkers also provided insight into the forms of nitrogen used by *Prochlorococcus*. Although phytoplankton, including *Prochlorococcus*, are often considered to prefer ammonia as a source of nitrogen (*21*), nitrite (*21*), nitrate (*22*), urea (*8*, *22*, *23*), and cyanate (*24*) have also been observed to be available to *Prochlorococcus*. In this study, the *Prochlorococcus* urea transporter protein (UrtA) was among the most abundant proteins that we detected with concentrations of 1000 to 2500 fmol $liter^{-1}$ in the North Pacific Subtropical Gyre (NPSG), comparable to that of the iron transporter IdiA in the iron-limited regions to the south, implying that dissolved organic nitrogen was an important nutritional source for *Prochlorococcus*. Biomarkers for a subunit of the urease enzyme (UreC) and an ammonia transporter (Amt1) from high-light *Prochlorococcus* showed meridional distributions similar to that of NtcA and the urea transporter, but both were found at much lower abundances compared to the urea transporter (fig. S5 and tables S3 and S4). Low urease abundance is likely related to the enzyme's efficiency relative to the challenge of acquiring scarce urea. This urea utilization could be a useful chemical and ecological strategy for high-light *Prochlorococcus* in ammonia-limiting waters, allowing direct acquisition of this zooplankton waste product without the need for a heterotrophic microbial intermediary with urease capability. The low concentrations of ammonia and urea transporters on the equator (station 5, fig. S5) could reflect the use of the more abundant nitrate and nitrite (*25*) (nitrite was 1.8 to 7.5 times more abundant than ammonia, and nitrate was 17 times more abundant than nitrite in the upper 100 m; figs. S6 and S15). Alternatively, the abundant ammonia concentrations could have induced low ammonia transporter concentrations, or another ammonia transporter sequence was in use that was not being targeted in our study since the targeted peptide was only identified in one *Prochlorococcus* isolate genome (table S4).

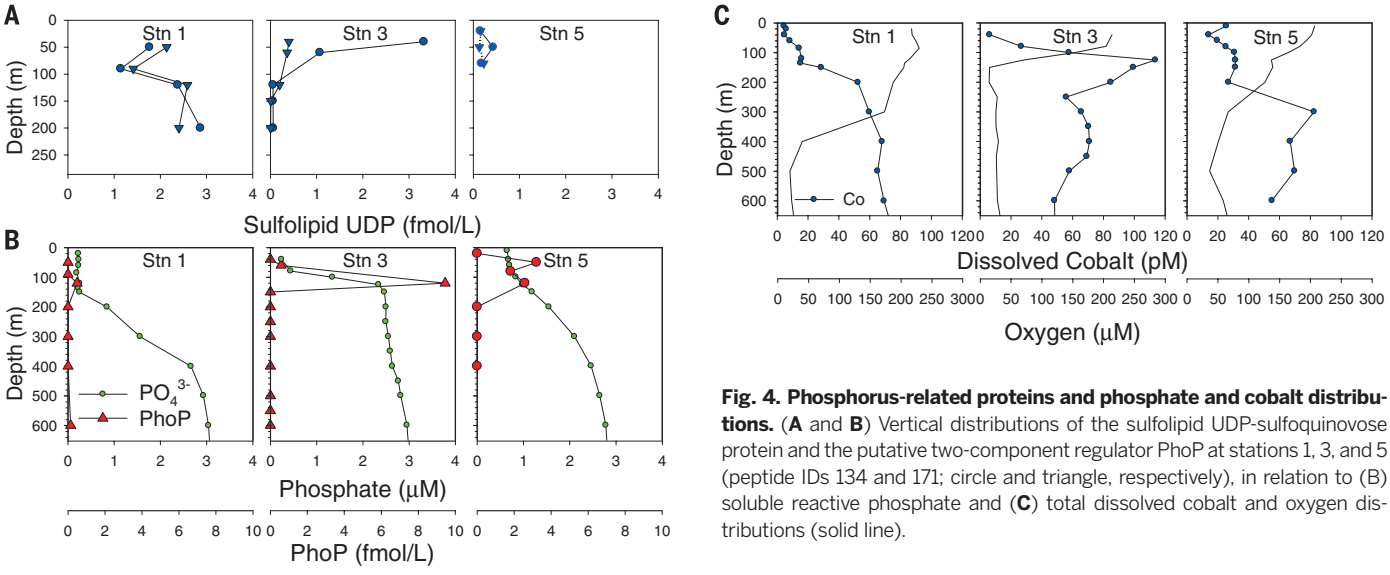

Fig. 4. Phosphorus-related proteins and phosphate and cobalt distributions. (**A** and **B**) Vertical distributions of the sulfolipid UDP-sulfoquinovose protein and the putative two-component regulator PhoP at stations 1, 3, and 5 (peptide IDs 134 and 171; circle and triangle, respectively), in relation to (B) soluble reactive phosphate and (**C**) total dissolved cobalt and oxygen distributions (solid line).

(Fig. 3C and fig. S7; IdiA, flavodoxin, NtcA, urea transporter, glutamine synthetase). Stations 3 and 9 had a considerable fraction of the nitrogen within this suite of five targeted proteins dedicated to the acquisition of both nutrients simultaneously (Fig. 3D and fig. S7, A and B). Although this estimate using selected proteins serves as a minimum nutritional estimate for the *Prochlorococcus* nitrogen and iron scarcity response, this analysis demonstrates that the community was deploying multiple nutrient acquisition strategies simultaneously, and hence was carrying the burden of an increased nutritional and energetic cost for maintaining both systems simultaneously as a potentially colimiting scenario. Moreover, although a previous study in a similar geographic region found that a novel low-iron ecotype dominated *Prochlorococcus* surface populations throughout (*27*), it is also possible that these biomarkers reflect an aggregated community signal of two or more coexisting high-light *Prochlorococcus* clades present in similar abundances. These results arguably present a challenge to current ecosystem parameterization influenced by Liebig's law of the minimum, where the required nutrient that is lowest in abundance relative to cellular requirements (e.g., cellular stoichiometry) solely controls growth rate by applying a minimum function to multiple Monod growth expression terms (*3*, *4*). Implicit in this minimum approach is an assumption that there is no metabolic or energetic penalty for the occurrence of more than one scarce nutrient simultaneously. Yet, these observations point to nutritional costs associated with maintaining the cellular machinery required to obtain a second scarce nutrient at the biomes' intersections.

Other nutrients, in addition to iron and nitrogen, were also scarce in this region and could influence primary productivity and community composition (*3*, *4*). Phosphorus and cobalt, in particular, are required for growth of *Prochlorococcus* (*28*, *29*) and were both highly depleted in the upper photic zone of the NPSG (Fig. 4, B and C). Two peptide biomarkers for the sulfolipid uridine 5-diphosphate (UDP) sulfoquinovose enzyme from high-light *Prochlorococcus* were found to be present at stations 1 and 3, but were diminished by station 5 as phosphate approached 1 μM in surface waters (Fig. 4A). *Prochlorococcus* uses this enzyme to replace phospholipids for sulfolipids as an adaptive response to phosphate scarcity (*30*). Deeper (low light) cyanobacterial communities responded to nutrient distributions along the transect. A protein homologous to the two-component phosphate response regulator PhoP in *Bacillus subtilis* (*31*) was identified during the metaproteome analyses (table S3) that corresponded to low-light *Prochlorococcus* ecotype and *Synechococcus* genomes (table S4). This two-component response regulator is one of seven identified in *Prochlorococcus* (*32*), yet was not previously observed to be responsive to phosphate scarcity (*29*). In this transect, this putative PhoP showed a similarity to the photic zone vertical distributions of phosphate and cobalt (Fig. 4), consistent with a role in regulation of phosphate metabolism near the nutricline. Notably, the expression of PhoP was opposite that of the two-component regulatory system PhoR identified in high-light *Prochlorococcus* ecotypes that is abundant under phosphate-scarcity rather than phosphate-replete conditions. PhoR is only present as a pseudogene in the low-light *Prochlorococcus* ecotype (*29*), implying that alternate response regulators such as PhoP are needed for regulation of low-light *Prochlorococcus* communities.

The distributions of the putative PhoP also resembled those of dissolved cobalt, whose distribution often correlates with that of phosphate (Fig. 4). Although cobalt is an essential micronutrient for *Prochlorococcus* and is the rarest of the metallic micronutrients in the sea (*28*), there are as yet no cyanobacterial biomarkers known to represent cobalt stress. The similarity to cobalt is also consistent with a metal requirement for the alkaline phosphatase enzyme, globally observed photic zone correlations of cobalt and phosphate (*33*), and several potential metal-related proteins within the gene neighborhood of *phoP* (including a transporter, protease, and carbonic anhydrase). Utilization of the micronutrient nickel also varied across the transect, yet in contrast to the low-abundance nickel-containing urease mentioned above, the nickel superoxide dismutase enzyme was highly abundant and increased in concentration toward the southern half of the transect, presumably in response to oxidative stress associated with iron-limiting physiology (fig. S6). Consistent with nickel superoxide dismutase being much more abundant than urease, the nickel measured in filtered particulate material was more abundant on the equatorial and southern regions of the transect (fig. S6).

These results show the utility of targeted metaproteomics in diagnosing nutrient stress of a major phytoplankton group, studying changes in ecological stoichiometry, and identifying novel regulatory components and their potential role in the systems biology of the oceans. Future climate is predicted to alter the oceanic biogeochemical provinces (*34*), with marine cyanobacterial populations expected to be affected, although it has been difficult to predict the nature of these impacts (*35*, *36*). Diagnostic measurements deployed over large geographic regions, such as the targeted metaproteomics methods shown here, could be valuable in characterizing the response to multiple influences.

REFERENCES AND NOTES

1. E. L. Mann, S. W. Chisholm, *Limnol. Oceanogr.* **45**, 1067–1076 (2000).
2. J. K. Moore, S. C. Doney, K. Lindsay, *Global Biogeochem. Cycles* **18**, GB4028 (2004).
3. C. M. Moore *et al.*, *Nat. Geosci.* **6**, 701–710 (2013).
4. M. A. Saito, T. J. Goepfert, J. T. Ritt, *Limnol. Oceanogr.* **53**, 276–290 (2008).
5. E. A. Webb, J. W. Moffett, J. B. Waterbury, *Appl. Environ. Microbiol.* **67**, 5444–5452 (2001).
6. D. Lindell, A. F. Post, *Appl. Environ. Microbiol.* **67**, 3340–3349 (2001).

7. S. M. Sowell *et al.*, *ISME J.* **3**, 93–105 (2009).
8. R. M. Morris *et al.*, *ISME J.* **4**, 673–685 (2010).
9. Materials and Methods are available on *Science* online.
10. G. Reygondeau *et al.*, *Global Biogeochem. Cycles* **27**, 1046–1058 (2013).
11. R. M. Gordon, K. H. Coale, K. S. Johnson, *Limnol. Oceanogr.* **42**, 419–431 (1997).
12. D. M. Karl, R. R. Bidigare, R. M. Letelier, *Deep Sea Res. Part II Top. Stud. Oceanogr.* **48**, 1449–1470 (2001).
13. F. Partensky, W. R. Hess, D. Vaulot, *Microbiol. Mol. Biol. Rev.* **63**, 106–127 (1999).
14. V. Lange *et al.*, *Mol. Cell. Proteomics* **7**, 1489–1500 7(2008).
15. J. LaRoche, P. W. Boyd, R. M. L. McKay, R. J. Geider, *Nature* **382**, 802–805 (1996).
16. A. W. Thompson, K. Huang, M. A. Saito, S. W. Chisholm, *ISME J.* **5**, 1580–1594 (2011).
17. D. Lindell, E. Padan, A. F. Post, *J. Bacteriol.* **180**, 1878–1886 (1998).
18. A. C. Tolonen *et al.*, *Mol. Syst. Biol.* **2**, 53 (2006).
19. G. Rocap, D. L. Distel, J. B. Waterbury, S. W. Chisholm, *Appl. Environ. Microbiol.* **68**, 1180–1191 (2002).
20. L. O. Slemons, J. W. Murray, J. Resing, B. Paul, P. Dutrieux, *Global Biogeochem. Cycles* **24**, GB3024 (2010).
21. L. R. Moore, A. F. Post, G. Rocap, S. W. Chisholm, *Limnol. Oceanogr.* **47**, 989–996 (2002).
22. J. R. Casey, M. W. Lomas, J. Mandecki, D. E. Walker, *Geophys. Res. Lett.* **34**, L10604 (2007).
23. B. Wawrik, A. V. Callaghan, D. A. Bronk, *Appl. Environ. Microbiol.* **75**, 6662–6670 (2009).
24. N. A. Kamennaya, A. F. Post, *Limnol. Oceanogr.* **58**, 1959–1971 (2013).
25. A. C. Martiny, S. Kathuria, P. M. Berube, *Proc. Natl. Acad. Sci. U.S.A.* **106**, 10787–10792 (2009).
26. G. R. DiTullio, D. A. Hutchins, K. W. Bruland, *Limnol. Oceanogr.* **38**, 495–508 (1993).
27. D. B. Rusch, A. C. Martiny, C. L. Dupont, A. L. Halpern, J. C. Venter, *Proc. Natl. Acad. Sci. U.S.A.* **107**, 16184–16189 (2010).
28. M. A. Saito, J. W. Moffett, S. W. Chisholm, J. B. Waterbury, *Limnol. Oceanogr.* **47**, 1629–1636 (2002).
29. A. C. Martiny, M. L. Coleman, S. W. Chisholm, *Proc. Natl. Acad. Sci. U.S.A.* **103**, 12552–12557 (2006).
30. B. A. S. Van Mooy, G. Rocap, H. F. Fredricks, C. T. Evans, A. H. Devol, *Proc. Natl. Acad. Sci. U.S.A.* **103**, 8607–8612 (2006).
31. S. M. Birkey, W. Liu, X. Zhang, M. F. Duggan, F. M. Hulett, *Mol. Microbiol.* **30**, 943–953 (1998).
32. I. Mary, D. Vaulot, *FEMS Microbiol. Lett.* **226**, 135–144 (2003).
33. A. E. Noble, M. A. Saito, K. Maiti, C. Benitez-Nelson, *Deep Sea Res. Part II Top. Stud. Oceanogr.* **55**, 1473–1490 (2008).
34. J. J. Polovina, J. P. Dunne, P. A. Woodworth, E. A. Howell, *ICES J. Mar. Sci.* **68**, 986–995 (2011).
35. P. W. Boyd, R. Strzepek, F. Fu, D. A. Hutchins, *Limnol. Oceanogr.* **55**, 1353–1376 (2010).
36. P. Flombaum *et al.*, *Proc. Natl. Acad. Sci. U.S.A.* **110**, 9824–9829 (2013).

ACKNOWLEDGMENTS

This work was made possible by NSF grants OCE-1031271, 1155566, and 1233261 Gordon Betty Moore Foundation grants 2724 and 3782, the Center for Microbial Research and Education, and the Woods Hole Oceanographic Institution Ocean Life Institute. We are grateful to the captain and crew of the R/V *Kilo Moana*, particularly V. Polidoro for his resourcefulness. We thank N. Hawco, D. Wang, and P. Balcom for sampling assistance and J. Dusenberry for programming assistance. We thank A. Santoro, J. Waterbury, and P. Chivers for helpful discussions and J. Blethrow and V. Zabrouskov (Thermo Scientific) for analyses on the prototype Fusion. Data for the Metyme Expedition are available at www.bco-dmo.org.

SUPPLEMENTARY MATERIALS

www.sciencemag.org/content/345/6201/1173/suppl/DC1
Materials and Methods
Supplementary Text
Figs. S1 to S18
Tables S1 to S6
References (*37*–*63*)

23 May 2014; accepted 25 July 2014
10.1126/science.1256450

PALEOCLIMATE

Greenland temperature response to climate forcing during the last deglaciation

Christo Buizert,[1]* Vasileios Gkinis,[2,3] Jeffrey P. Severinghaus,[4] Feng He,[5] Benoit S. Lecavalier,[6] Philippe Kindler,[7] Markus Leuenberger,[7] Anders E. Carlson,[1] Bo Vinther,[2] Valérie Masson-Delmotte,[8] James W. C. White,[3] Zhengyu Liu,[5,9] Bette Otto-Bliesner,[10] Edward J. Brook[1]

Greenland ice core water isotopic composition ($\delta^{18}O$) provides detailed evidence for abrupt climate changes but is by itself insufficient for quantitative reconstruction of past temperatures and their spatial patterns. We investigate Greenland temperature evolution during the last deglaciation using independent reconstructions from three ice cores and simulations with a coupled ocean-atmosphere climate model. Contrary to the traditional $\delta^{18}O$ interpretation, the Younger Dryas period was 4.5° ± 2°C warmer than the Oldest Dryas, due to increased carbon dioxide forcing and summer insolation. The magnitude of abrupt temperature changes is larger in central Greenland (9° to 14°C) than in the northwest (5° to 9°C), fingerprinting a North Atlantic origin. Simulated changes in temperature seasonality closely track changes in the Atlantic overturning strength and support the hypothesis that abrupt climate change is mostly a winter phenomenon.

The last deglaciation [~19 thousand to 11 thousand years before the present (ky B.P.)] is the most recent example of natural global warming and large-scale climate reorganization, providing an exceptional opportunity to study the interaction between different components of the climate system (*1*) and climate sensitivity to changes in radiative forcing (*2*). Much of the regional and global climate variability of this period can be explained as the superposition of two distinct modes (*3*, *4*): a global increase in surface temperature related to increased radiative forcing (Fig. 1C) and an interhemispheric redistribution of heat associated with variability in the Atlantic meridional overturning circulation (AMOC) strength (Fig. 1D).

High-resolution records of Northern Hemisphere (NH) high-latitude climate are provided by Greenland ice core water isotopic composition ($\delta^{18}O$ and δD), a proxy for local condensation temperature (Fig. 1A). Past water isotopic variations reflect site temperature (T_{site}) to first order (*5*) but are also influenced by changes to the atmospheric hydrological cycle, such as evaporation conditions (*6*, *7*), moisture origin and transport pathways (*8*, *9*), and precipitation intermittency or seasonality (*10*). Assuming a linear $\delta^{18}O$-T_{site} relationship suggests that Greenland climate did not begin to warm until the Bølling onset (14.7 ky B.P.), lagging much of the globe and implying a negligible Greenland temperature response to increasing atmospheric CO_2 (*11*–*14*). Such delayed Arctic warming is hard to reconcile with past sea levels and NH ice sheet extent that indicate substantial ice loss before the Bølling (*15*). This paradox is exemplified by lower Greenland summit $\delta^{18}O$ levels during the Younger Dryas period (YD, 12.8 to 11.7 ky B.P.) than during the Oldest Dryas period (OD, 18 to 14.7 ky B.P.), despite the rise in boreal summer insolation (Fig. 1B) and a ~50 parts per million increase in atmospheric CO_2 (*14*, *16*).

Accurate temperature reconstructions are required to improve our understanding of the mechanisms controlling Greenland climate during the last deglaciation and to benchmark transient climate simulations (*17*, *18*). Here, we circumvent the issues that confound water isotope interpretation by using four independent temperature reconstructions from three ice cores

[1]College of Earth, Ocean, and Atmospheric Sciences, Oregon State University, Corvallis, OR 97331, USA. [2]Centre for Ice and Climate, Niels Bohr Institute, University of Copenhagen, Denmark. [3]Institute of Arctic and Alpine Research, University of Colorado, Boulder, CO 80309, USA. [4]Scripps Institution of Oceanography, University of California–San Diego, La Jolla, CA 92093, USA. [5]Center for Climatic Research, Nelson Institute for Environmental Studies, University of Wisconsin, Madison, WI 53706, USA. [6]Department of Physics and Physical Oceanography, Memorial University, St. John's, Canada. [7]Division of Climate and Environmental Physics, Physics Institute and Oeschger Centre for Climate Change Research, University of Bern, Bern, Switzerland. [8]Laboratoire des Sciences du Climat et de l'Environnement, Institut Pierre Simon Laplace (UMR CEA-CNRS-UVSQ 8212), Gif-sur-Yvette, France. [9]Laboratory for Climate and Ocean-Atmosphere Studies, Peking University, Beijing 100871, China. [10]Climate and Global Dynamics Division, National Center for Atmospheric Research, Boulder, CO 80307, USA.
***Corresponding author. E-mail: buizertc@science.oregonstate.edu**